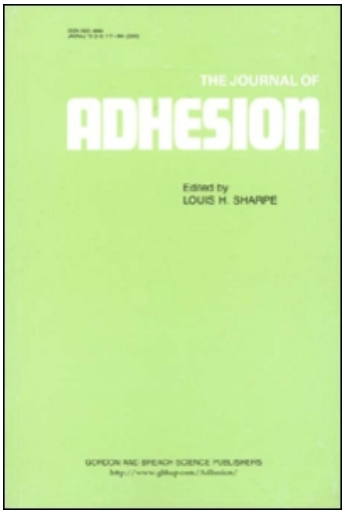

The Journal of Adhesion
Publication details, including instructions for authors and subscription information:
http://www.informaworld.com/smpp/title~content=t713453635

How Compliance Compensates for Surface Roughness in Fibrillar Adhesion

C. -Y. Hui[a]; N. J. Glassmaker[b]; A. Jagota[b]
[a] Cornell University, Ithaca, New York, USA [b] Lehigh University, Bethlehem, Pennsylvania, USA

To cite this Article Hui, C. -Y. , Glassmaker, N. J. and Jagota, A.(2005) 'How Compliance Compensates for Surface Roughness in Fibrillar Adhesion', The Journal of Adhesion, 81: 7, 699 — 721
To link to this Article: DOI: 10.1080/00218460500187673
URL: http://dx.doi.org/10.1080/00218460500187673

The Journal of Adhesion, 81:699–721, 2005

ISSN: 0021-8464 print/1545-5823 online
DOI: 10.1080/00218460500187673

Taylor & Francis
Taylor & Francis Group

How Compliance Compensates for Surface Roughness in Fibrillar Adhesion

C.-Y. Hui
Cornell University, Ithaca, New York, USA

N. J. Glassmaker
A. Jagota
Lehigh University, Bethlehem, Pennsylvania, USA

Fibrillar interfaces play an important role in the ability of many small animals to adhere to surfaces. Surface roughness is generally deleterious to adhesion because it hinders the ability of mating surfaces to make contact, but fibrillar surfaces compensate for surface roughness by virtue of their enhanced compliance. We examine the relationship between roughness and compliance by analyzing the mechanics of detaching an array of fibrils from a substrate. The theory of Johnson, Kendall, and Roberts is used to describe the interfacial adhesion of each fibril, and roughness is modeled by making the fibril length a random variable subject to a probability distribution. We solve for the mean force response of a fibrillar array as a function of the displacement of the entire array. From these results we extract the mean fibrillar pull-off force and work to separate the fibrillar array and substrate. We show how the mean fibrillar pull-off force decreases with increasing roughness-height standard deviation: the relationship is linear for small height standard deviation, and the pull-off force trails off to zero for very rough surfaces. Conversely, the work of separation is shown to be unaffected by small roughness-height standard deviation, although it decreases toward zero for rougher surfaces. The effects of roughness may be offset by increasing fibrillar compliance; for small roughness-height standard deviation, we show that the reduction in pull-off force is inversely proportional to the normalized compliance. We also show that the work of separation increases linearly with the compliance when the compliance is large compared with the roughness-height standard deviation.

Keywords: Adhesion; Compliance; Fibrillar interface; Setae; Surface roughness

Received 22 October 2004; in final form 28 February 2005.

One of a collection of papers honoring Manoj K. Chaudhury, the February 2005 recipient of The Adhesion Society Award for Excellence in Adhesion Science, sponsored by 3M.

Address correspondence to Nicholas J. Glassmaker, Department of Chemical Engineering, Lehigh University, Iacocca Hall 111, Research Drive, Bethlehem, PA 18015, USA. E-mail: nicholas@lehigh.edu

INTRODUCTION

A number of recent studies have explored the mechanics of fibrillar interfaces [1–4], which are commonly found in small animals as friction or adhesion promoters (see, *e.g.*, [2, 5–7]). Among these studies, the results of several interesting calculations suggest that interfacial arrays of small length scale fibrils ($\leq 5\,\mu$m in diameter) can possess greater failure strength and/or toughness than corresponding flat interfaces [1, 2, 4, 8]. An additional benefit of the fibrillar geometry is its ability to arrest interfacial crack propagation by eliminating crack-like stress concentrations and promoting a more uniform distribution of load sharing among fibrils [4, 8]. Moreover, because of an effective increase in surface compliance, fibrillar interfaces are expected to be able to make contact with and adhere to a variety of surfaces with varying degrees of roughness [1, 3]. This is important to biological adhesion, because animals in their natural habitats encounter many types of surfaces, each with its own roughness characteristics.

Many conventional adhesives suffer a reduction in adhesion when they make contact with a rough surface. For example, pressure-sensitive adhesives are ineffective on nonsmooth surfaces and are easily fouled by particulates. On the other hand, a fibrillar surface should be more capable of maintaining its contact and adhesion properties against rough surfaces, even for high modulus materials. Persson has quantified some important aspects of this problem and determined the work necessary to fail a fibrillar interface in the presence of roughness [1]. He found that the work to fail a fibrillar contact array decreases with an increase in roughness-height variation. In his article, however, the pull-off force is left as a parameter, so that it is difficult to judge the role of compliance. Similarly, Greenwood and Williamson have studied adhesive contact of a rough surface with random asperities to a smooth hard substrate [9], but, in their model, the asperities are not backed by fibrils, so the role of fibrillar compliance is not clear.

Here, we choose a particular model for the interfacial adhesion (the theory of Johnson, Kendall, and Roberts [10], JKR), which allows us to characterize the role of compliance more carefully. In addition, the model is simple enough that we are able to obtain closed-form results for the limit of small roughness-height standard deviation. We note that the JKR theory is only an approximate model for most biological fibrillar-adhesion systems, because fibrils in these systems typically have plate-like "spatular" ends [5–7, 11]. The JKR geometry, conversely, is best suited for convex, *e.g.*, spherical, contacts. As a result,

it is almost certain that the JKR theory will be inaccurate in modeling the force-displacement response of biological fibrils over some range of displacement.

Nevertheless, Arzt *et al*. have shown that the JKR theory describes the net adhesion force of the terminal elements of biological fibrils quite well for many species of animals [2]. In particular, they showed that JKR adhesion-force scaling is consistent with the scaling of setal diameter in organisms of vastly different body mass. Because of this, we use the JKR theory in spite of its limitations and expect the results to be indicative, if not precisely predictive, of the behavior of biological fibrillar adhesion. Moreover, we note that our results may be more generally applicable in technological applications where the JKR contact theory is more appropriate, *i.e*., biomimetic fibrillar interfaces with rounded, approximately spherically ended fibrils.

To complement Persson's energy calculation mentioned previously, we determine here the mean fibrillar load as a function of the surface separation. In particular, we find how the tensile pull-off load depends on the spring compliance and material properties as well as the roughness-height standard deviation. Also, we determine the work of separation as a function of the same parameters for our particular choice of JKR as the adhesion model.

The structure of the article is as follows: Specific aspects of the model are presented in the next section, "Problem Formulation." In our model, we use the JKR force-displacement relationship to describe contact between fibrils of random length and a flat substrate; the randomness in fibril length is our way of approximating a rough surface. After manipulating the governing equations, we show that the average fibrillar force may be expressed in terms of the net displacement of the fibrillar array through the evaluation of an integral. In the "Results" section, we present the results of our calculations, which are largely graphical because the integral for the average fibrillar force must be evaluated numerically. We interpret the force-displacement response of the fibrillar array in terms of the two important adhesion-performance quantities mentioned previously: the maximum tensile pull-off stress and the work of separation. Finally, before concluding, we discuss the relevance of our results to biological fibrillar-adhesion systems and synthetic mimics of the same.

PROBLEM FORMULATION

To examine our notions about roughness systematically, we consider the mechanical model of a fibrillar surface shown in Figure 1. Each fibril consists of an elastic spring and hemispherical end. The linear

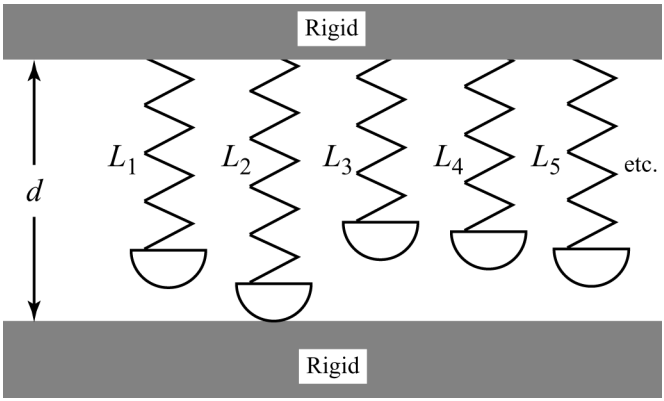

FIGURE 1 Schematic illustration of an array of nonuniform length fibrils.

springs represent the fact that the fibrils have some nonzero compliance

$$C \approx \overline{L}/(\pi E R^2) \tag{1}$$

for cylindrical fibrils oriented perpendicularly to their backing. Here, $\overline{L}$ is the mean fibril length, E is the elastic modulus, and R is the fibril radius (assumed equal to the hemisphere radius). Note that if the fibrils are inclined at an angle other than 90°, then the compliance is considerably enhanced and one can use beam theory to obtain its value. For example, if the fibrils are oriented at an angle θ to the backing, then

$$C \approx \overline{L} \sin\theta[1 + 4\overline{L}^2/(3R^2)\cot^2\theta]/(\pi E R^2). \tag{2}$$

(See Reference [3] for a derivation.)

Nominally, all fibrils have the same compliance, because we use the mean length when calculating it. However, the fibrils do vary in length, and we describe this using a statistical distribution. Although we explicitly treat the case of variable fibril length against a flat surface, if the variation in length is small compared with the mean length, as expected physically, our results can be applied to the case when variability arises because of surface roughness or both surface roughness and length.* Alternatively, our results should also be valid

*Note that when fabricating synthetic fibrillar structures, it is likely that fibril length across the array will not be perfectly uniform, even though the roughness of the opposing adherend may be insignificantly small. Since van der Waals interactions are quite short ranged (~2 nm), these apparently small variations in fibril length will have significant effect on the pull-off force and effective toughness.

when the roughness profile has height variation on the order of the fibril length if the roughness wavelength is on the same order as the fibril separation.

To begin the formulation, define the deflection of the ith fibril Δ_i as

$$\Delta_i \equiv d - L_i, \tag{3}$$

where d is the surface separation shown in Figure 1.

As discussed previously, we model the contact between the fibrils' hemispherical ends and the substrate using the JKR theory. From the JKR theory, we know that for a load-controlled test, pull-off occurs when the load reaches a critical tensile value

$$P_c = -\frac{3}{2}\pi R W, \tag{4}$$

where R is the radius of the hemisphere and W is the work of adhesion between the surfaces. When the load reaches this value, the JKR theory specifies the displacement of points far from the contact zone, δ_c, and contact radius, a_c, to be

$$\delta_c = -\left(\frac{3R}{4}\right)^{1/3}\left(\frac{\pi W}{4E^*}\right)^{2/3} \tag{5}$$

and

$$a_c = \left(\frac{3R}{4}\right)^{2/3}\left(\frac{2\pi W}{E^*}\right)^{1/3}, \tag{6}$$

where $E^* = E/(1-\nu^2)$, for a material with Young's modulus, E, and Poisson's ratio, ν. (see Reference [10] for derivations of Equations (4)–(6).)

Thus, if a fibril is at the instant of pull off,

$$\Delta_c = -CP_c - \delta_c. \tag{7}$$

That is, for $\Delta_i > \Delta_c$, the load on the ith fibril becomes zero. We are interested in situations where $\Delta_i \leq \Delta_c$, *i.e.*, when the fibril is in contact and bears load. In this case,

$$\Delta_i = -CP_i - \delta_i, \tag{8}$$

where C is the compliance of the spring, and the load, P_i, and displacement, δ_i, are

$$P_i = \frac{4E^* a_i^3}{3R} - 2a_i^{3/2}\sqrt{2\pi E^* W} \tag{9}$$

and

$$\delta_i = \frac{a_i^2}{R} - \sqrt{\frac{2\pi W a_i}{E^*}}, \tag{10}$$

according to the JKR theory [10]. Henceforth, we dispense with the subscript i notation with the understanding that P, δ, a, and Δ are quantities associated with single fibrils.

We consider the length of a fibril to be a random variable, described by the probability density function $p(L)$. Thus, the mean length is given by

$$\overline{L} = \int_0^\infty p(L) L dL. \tag{11}$$

Furthermore, if we can find the function $f_P(L)$, which expresses the load P on a fibril as a function of L, then the mean fibrillar load is

$$\overline{P} = \int_0^\infty p(L) f_P(L) dL. \tag{12}$$

This is the important quantity for understanding the contact mechanics of our array of fibrils of nonuniform length. Indeed, the stress the fibrillar array supports is just $\overline{P}$ times the fibrillar areal density. Thus, let us proceed to calculate $\overline{P}$.

From Equations (3) and (8), it is clear that

$$P = (L - d - \delta)/C, \tag{13}$$

However, because δ is also an unknown function of L, this does not explicitly provide the desired $f_P(L)$. Instead of trying to determine this function, let us rather change the integration variable in Equation (12) to the contact radius, a. Substituting Equations (9) and (10) in (13), one obtains

$$L = d + \frac{a^2}{R} - \sqrt{\frac{2\pi W a}{E^*}} + C\left(\frac{4E^* a^3}{3R} - 2a^{3/2}\sqrt{2\pi E^* W}\right), \tag{14}$$

so that

$$dL = \left[\frac{2a}{R} - \sqrt{\frac{\pi W}{2E^* a}} + C\left(\frac{4E^* a^2}{R} - 3a^{1/2}\sqrt{2\pi E^* W}\right)\right] da. \tag{15}$$

We can use Equation (9) to express P as a function of a in the integrand of Equation (12), rather than trying to find $f_P(L)$. Then, given the probability-density function, we can merely substitute Equation

(14) to get the entire integrand to be a function of a. For the limits of integration, the upper limit remains the same but the lower limit changes to a_c, because the fibril supports no load for $a \leq a_c$[†] and negative contact radii are not possible.

To illustrate our model, let us assume the fibril lengths are normally distributed. In this case,

$$p(L) = \frac{1}{\sqrt{2\pi}s} \exp\left[-(L - \overline{L})^2/(2s^2)\right], \tag{16}$$

where $\overline{L}$ is the mean fibril length and s is the standard deviation. Using Equations (9) and (14)–(16), we can express the integral in Equation (12) entirely in terms of a.

Before doing this, let us first normalize the equations using

$$\begin{aligned} &\widetilde{P} = P/|P_c|,\ \tilde{a} = a/a_c,\ \tilde{\delta} = \delta/|\delta_c|,\ \widetilde{L} = L/|\delta_c|, \\ &\tilde{s} = s/|\delta_c|,\ \widetilde{D} = (d - \overline{L})/|\delta_c|. \end{aligned} \tag{17}$$

The JKR Equations (9) and (10) become

$$\widetilde{P} = \tilde{f}(\tilde{a}) \equiv \tilde{a}^3 - 2\tilde{a}^{3/2} \tag{18}$$

and

$$\tilde{\delta} = \tilde{g}(\tilde{a}) \equiv 3\tilde{a}^2 - 4\tilde{a}^{1/2}. \tag{19}$$

Furthermore, Equation (15) becomes

$$d\widetilde{L} \equiv \tilde{h}(\tilde{a})d\tilde{a} = \left[3\widetilde{C}(\tilde{a}^2 - \tilde{a}^{1/2}) + 2(3\tilde{a} - \tilde{a}^{-1/2})\right]d\tilde{a}, \tag{20}$$

where

$$\widetilde{C} \equiv \frac{C|P_c|}{|\delta_c|} = 6\pi C\left(\frac{(E^*R)^2W}{3\pi^2}\right)^{1/3}. \tag{21}$$

Note here the physical significance of the normalized compliance, $\widetilde{C}$: it is the ratio of the compliance of the fibril to the intrinsic compliance of the attachment. The intrinsic compliance of the attachment is controlled by the flexibility of the contacting ends or "spatula" [5, 11] for animal setae. Continuing, substitution of the normalized forms of

[†]This analysis assumes each fibril fails in load control. Because we are primarily interested in highly compliant fibrils, this is an excellent assumption. If, however, C is very small, then the fibrils will continue to sustain a decreasing load until a different (smaller) a_c is reached. More on this in the discussion section.

Equations (9) and (14)–(16) in equation (12) gives

$$\overline{\overline{\widetilde{P}}} = \frac{1}{\sqrt{2\pi}\tilde{s}} \int_1^\infty \exp\left[-\left(\widetilde{D} + \widetilde{C}\tilde{f}(\tilde{a}) + \tilde{g}(\tilde{a}) \right)^2 \left(2\tilde{s}^2\right)^{-1} \right] \tilde{f}(\tilde{a})\tilde{h}(\tilde{a}) d\tilde{a}. \quad (22)$$

We evaluated this integral numerically, and results are shown in Figures 2 and 3. Before continuing with a discussion of these results, we should comment on a few of our assumptions in this analysis. Strictly speaking, our solution is valid only if all fibrils are initially brought into contact and then pulled off. Because some compression is required for initial contact, the tensile (adhesion) force our model predicts may be overestimated if this is not the case. On the other hand, because in Equations (4)–(6) we require fibrils to fail at the JKR critical load for a load-controlled test, we may slightly underestimate the adhesion in situations of displacement control. (Some of the fibrils at the verge of failure in load control will continue to carry load for a short time longer in displacement control.) We expect both of these effects to be minor and not to alter any of our results significantly.

DISCUSSION

Numerical Results

The plots in Figure 2 show the mean fibrillar load, $\overline{\overline{\widetilde{P}}}(\widetilde{D})$, as calculated from Equation (22) via numerical quadrature for several values of the parameters $\tilde{s}$ and $\widetilde{C}$. Recall that $\widetilde{D}$ is the normalized distance separating the fibrillar array from the substrate, whereas $\tilde{s}$ is the normalized standard deviation in the fibril-height distribution and $\widetilde{C}$ is the normalized fibrillar compliance. The curves in Figure 2 should be interpreted as the average force per fibril resisting separation after the two surfaces have been compressed against each other sufficiently so that all fibrils are initially in contact. With increasing separation, $\widetilde{D}$, the initially compressive force[‡] (positive $\overline{\overline{\widetilde{P}}}$) passes through zero and turns tensile (negative $\overline{\overline{\widetilde{P}}}$) for all cases in Figure 2. The value of $\widetilde{D}$ at which $\overline{\overline{\widetilde{P}}}$ is first zero, $\widetilde{D}^*$, is the separation at which the interface rests when not subject to external loading. With further increase in $\widetilde{D}$, the force becomes negative, increases in magnitude until a maximum tension is attained, and then decreases, eventually to zero at full separation of the interface.

[‡]Note that in Figure 2, we plot $-\overline{\overline{\widetilde{P}}}$ rather than $\overline{\overline{\widetilde{P}}}$. Thus, *in the plots*, tensile forces plot as positive numbers, which is the usual convention in solid mechanics. Note, however, that throughout the article (and in the plots), forces are actually tensile when they have negative values and compressive when they have positive values, which is the standard convention in contact-mechanics calculations.

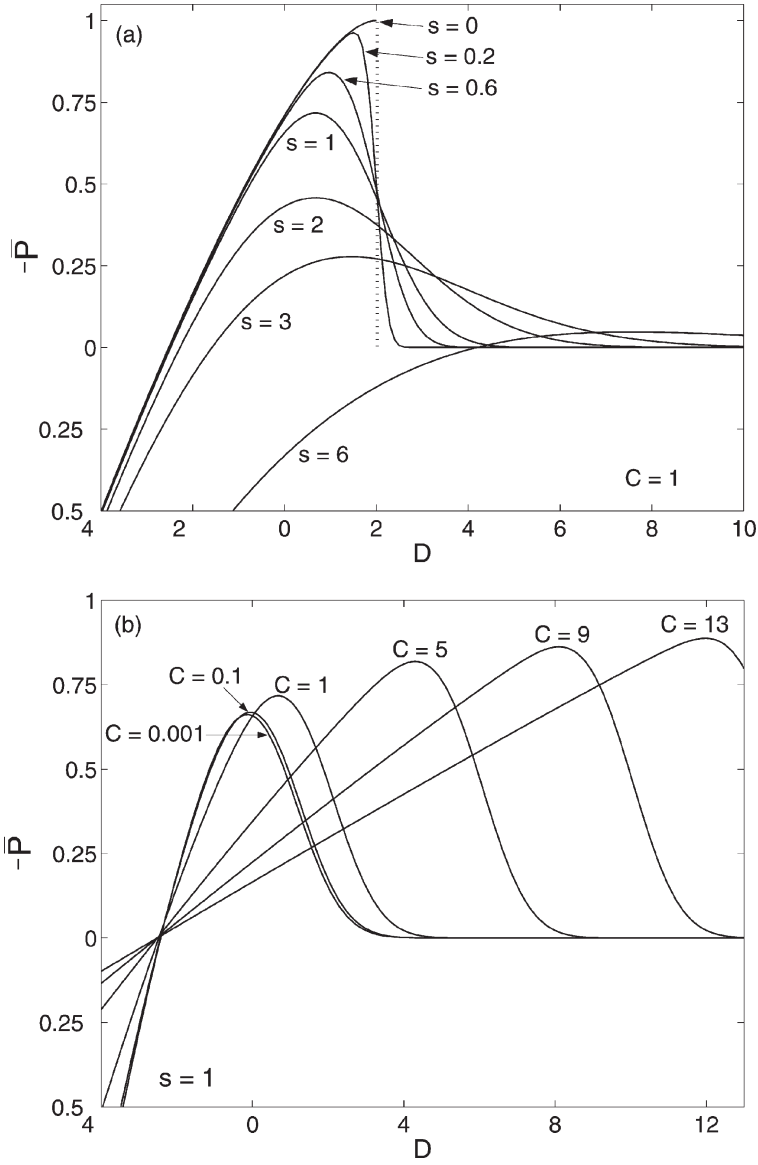

FIGURE 2 Plots of the mean load, $\bar{\bar{P}}$, as a function of the surface separation, $\tilde{D}$: (a) fixed compliance $\tilde{C}$, varying standard deviation of fibril length $\tilde{s}$ and (b) fixed standard deviation $\tilde{s}$, varying compliance $\tilde{C}$. All quantities in the plots are normalized; see text for definitions.

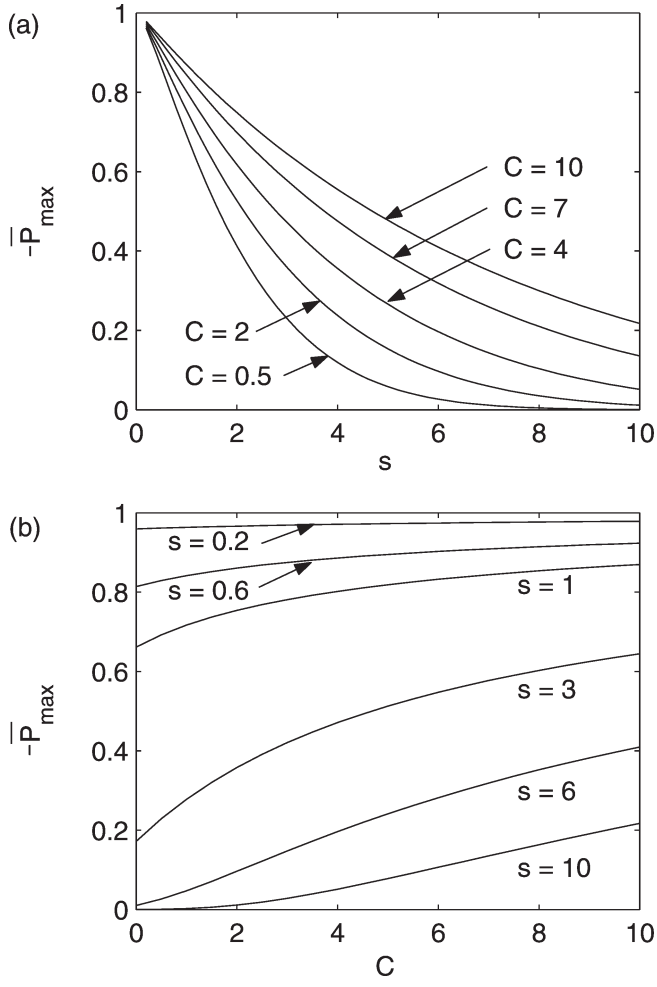

FIGURE 3 Plots of the mean tensile pull-off load $|\overline{\overline{P}}_{\max}|$ versus fibril compliance, $\tilde{C}$, and fibril height standard deviation, $\tilde{s}$: (a) contours of constant $\tilde{C}$, (b) contours of constant $\tilde{s}$, and (c) a plot of the full failure surface combining the information in (a) and (b). All quantities in the plots are normalized; see text for definitions.

Measures of Adhesion Performance

Two important pieces of information that one can extract from the $\overline{\overline{P}}(\widetilde{D})$ curves are (a) the peak tensile pull-off stress, equal to

$$\Sigma P_c |\overline{\overline{P}}_{\max}|, \tag{23}$$

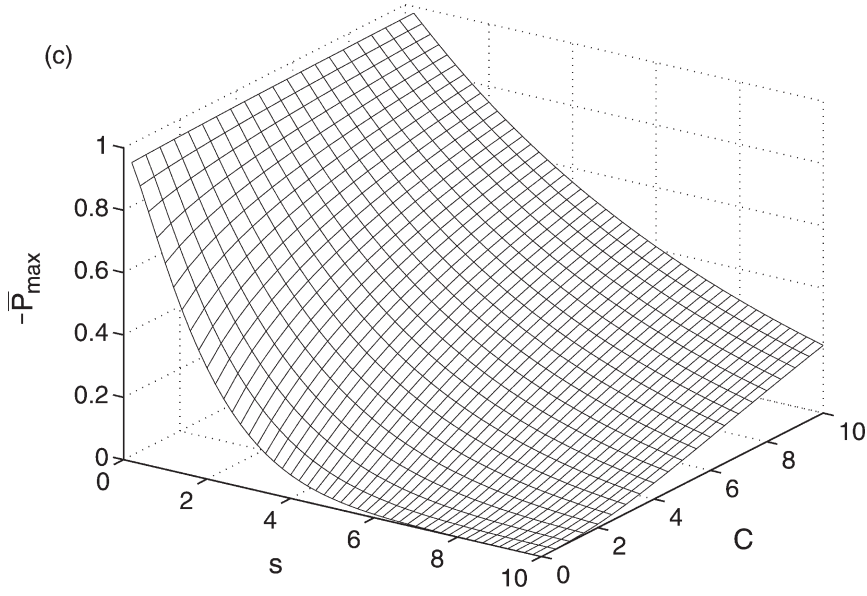

FIGURE 3 Continued.

which is the strength of the interface, and (b) the work of separation

$$\widetilde{U} \equiv U/(\pi W/2) \equiv \widetilde{\Sigma} \int_{\widetilde{D}^*}^{\infty} \overline{\widetilde{P}}(\widetilde{D}) d\widetilde{D}, \tag{24}$$

which is the toughness of the interface. Here, Σ is the fibrillar areal density, $\widetilde{\Sigma} \equiv \Sigma |a_c|^2$, and W is the intrinsic work of adhesion defined previously. Taking this integral to represent the toughness of the interface incorporates the assumption that when a fibril detaches, all its stored elastic energy is lost. We have argued for this assumption in other work. (See References [4, 8].)

The mean fibrillar pull-off force $|\overline{\widetilde{P}}_{max}|$ is shown in Figure 3, and the work of separation $\widetilde{U}/\widetilde{\Sigma}$ is shown in Figure 4. The $|\overline{\widetilde{P}}_{max}|$ values in Figure 3 are obtained by finding the peak tensile value of $\overline{\widetilde{P}}(\widetilde{D})$ from curves like those shown in Figure 2, and the work of separation is obtained by numerically integrating the same curves, as per Equation (24). Recall that in Equation (24) the lower limit, $\widetilde{D}^*$, is just the value of $\widetilde{D}$ where $\overline{\widetilde{P}}$ is first zero when pulling the fibrillar array out of compression. Also, although the upper limit is infinity, in practice we integrated the $\overline{\widetilde{P}}(\widetilde{D})$ curves until $\overline{\widetilde{P}}$ decayed to zero.

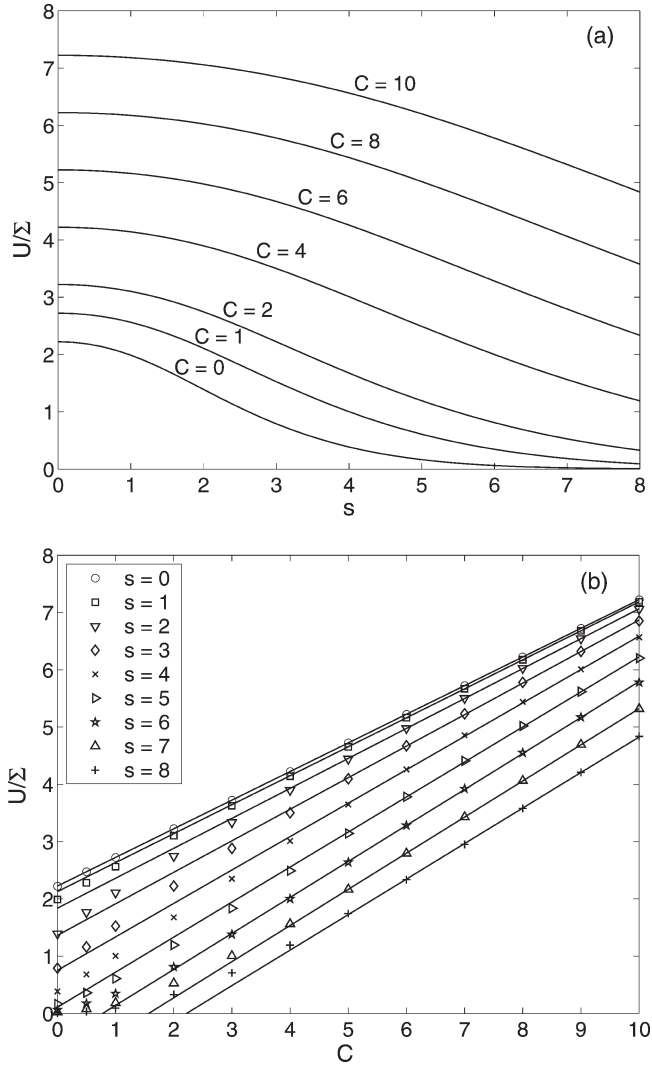

FIGURE 4 Plots of the separation energy, $\widetilde{U}/\widetilde{\Sigma}$, as a function of the fibril compliance, $\widetilde{C}$, and fibril height standard deviation, $\tilde{s}$. In (a), the curves are results of numerical quadrature calculations. In (b), only the data points are results of numerical calculations. The lines in (b) are the best linear fits to each set of data points. All quantities in the plots are normalized; see text for definitions.

In Figures 3 and 4, we see that the normalized measures of adhesion performance, $|\widetilde{\overline{P}}_{\max}|$ and $\widetilde{U}/\widetilde{\Sigma}$, are functions of only two normalized parameters: the standard deviation in fibril height

(*i.e.*, in roughness height), $\tilde{s}$, and the fibrillar compliance, $\widetilde{C}$. This should also be clear from Equations (18)–(20) and (22) and the definitions of $|\overline{\overline{P}}_{\max}|$ and $\widetilde{U}/\widetilde{\Sigma}$. The coarsest conclusion of this study clearly emerges from an inspection of Figures 3 and 4: both $|\overline{\overline{P}}_{\max}|$ and $\widetilde{U}/\widetilde{\Sigma}$ decrease with increasing $\tilde{s}$ and increase with increasing $\widetilde{C}$. That is, the strongest adhesion results for compliant fibrils attached to approximately flat surfaces, whereas the weakest adhesion results for stiff fibrils attached to rough surfaces. We refine this statement in the next two sections by considering some details of the features of these trends.

For example, examination of Figure 4a reveals that for small roughness-height deviation, $\tilde{s}$, the work of separation remains approximately constant. It then drops off toward zero at larger $\tilde{s}$. This is in stark contrast to the results for pull-off force, which decreases most quickly at small $\tilde{s}$. (See Figure 3a and c.) This identifies an important aspect of fibrillar adhesion in the presence of roughness: although a small amount of roughness does not significantly change the work necessary to fail the interface, it dramatically reduces the force necessary to accomplish it. This is physically sensible, because in our model, for small $\tilde{s}$, all fibrils still must follow approximately the same JKR P–δ failure curve. Thus, the total work does not change. However, the fibrils fail at different instants, when $\tilde{s} > 0$, which quickly reduces the pull-off force. When $\tilde{s}$ becomes larger, the amount of initial compression in each spring varies significantly from fibril to fibril, so that the P–δ failure curve is significantly different from fibril to fibril. As a result, even the work of separation is reduced at large $\tilde{s}$, as we see in Figure 4a. Having now a qualitative understanding of the behavior of the solution at small $\tilde{s}$, let us turn to some quantitative statements about the behavior of the solution in this and another important limit.

Approximations to the Solution in Several Limits

In Figure 3a, we observe another interesting feature of the solution: the mean pull-off load decreases approximately linearly in $\tilde{s}$ for small $\tilde{s}$. To understand this result, we consider an approximation for $\overline{\overline{P}}(\widetilde{D})$ when $\tilde{s}$ is small. As $\tilde{s} \to 0$, all fibrils will fail at the same load and displacement,

[§]Note that the mean pull-off load is limited by the JKR pull-off load, which is why $|\overline{\overline{P}}\max|$ never exceeds one. It can equal one only when all fibrils fail simultaneously, which, for finite compliance, happens only when there is no roughness, *i.e.*, when, $\tilde{s} \to 0$, as we see in Figure 3. As an aside, there is no limit to the separation energy. Indeed, because the elastic strain energy stored in the fibrils is considered to be part of the energy lost during separation by the definition of $\widetilde{U}/\widetilde{\Sigma}$ in Equation (24), $\widetilde{U}/\widetilde{\Sigma} \to \infty$ as $\widetilde{C} \to \infty$.

that is, when $\delta = \delta_c$ and $P = P_c^{\delta}$; this corresponds to the point $\widetilde{D} = \widetilde{C} + 1$. (See Equations (3) and (7).) One can show that near this point

$$\overline{\widetilde{P}}(\widetilde{D}) \approx \overline{\widetilde{P}}_1(\widetilde{D}) \equiv -\frac{1}{2}\operatorname{erfc}\left(\frac{\widetilde{D} - \widetilde{C} - 1}{\sqrt{2}\tilde{s}}\right). \tag{25}$$

(See Appendix 1.) Furthermore, when $\widetilde{D} << \widetilde{C} + 1$ (strong compression),

$$\overline{\widetilde{P}}(\widetilde{D}) \approx \overline{\widetilde{P}}_2(\widetilde{D}) \equiv -\widetilde{D}/\widetilde{C} + \mu, \tag{26}$$

where μ is a constant. Equation (26) is essentially a restatement of Equation (13) in the limit $\widetilde{D} << \widetilde{C} + 1$. Note that in this limit, $\tilde{\delta} \propto \widetilde{P}^{2/3}$, so that Equation (26) is correct as long as $\widetilde{C}$ is of order 1 or greater. (If $\widetilde{C}$ is less than order 1, then one cannot neglect the δ term in Equation (13).) To determine the constant μ, let us enforce the condition

$$\overline{\widetilde{P}}_2(\widetilde{D} = \widetilde{C} + 1) = -1, \tag{27}$$

which is a better and better approximation as $\tilde{s} \to 0$. One obtains $\mu = 1/\widetilde{C}$. Furthermore, the first two terms of the power series for $\overline{\widetilde{P}}_1(\widetilde{D})$ near $\widetilde{D} = \widetilde{C} + 1$ are

$$\overline{\widetilde{P}}_1(\widetilde{D}) \approx -\frac{1}{2} + \frac{\widetilde{D} - \widetilde{C} - 1}{\sqrt{2\pi}\tilde{s}}. \tag{28}$$

Now $\overline{\widetilde{P}}_1(\widetilde{D})$ and $\overline{\widetilde{P}}_2(\widetilde{D})$ represent a bilinear approximation to $\overline{\widetilde{P}}(\widetilde{D})$ for all $\widetilde{D} < \widetilde{C} + 1$. The maximum tensile load occurs where $\overline{\widetilde{P}}_1(\widetilde{D}) = \overline{\widetilde{P}}_2(\widetilde{D})$, that is, when

$$\widetilde{D} = \frac{1}{2}\left(\frac{\widetilde{C}^2}{\widetilde{C} + \sqrt{2\pi}\tilde{s}} + \widetilde{C} + 2\right). \tag{29}$$

Thus, the maximum tensile load is given by

$$\overline{\widetilde{P}}_{\max} \approx -1 + \frac{\sqrt{2\pi}\tilde{s}}{2(\sqrt{2\pi}\tilde{s} + \widetilde{C})} \approx -1 + \sqrt{\frac{\pi}{2}}\frac{\tilde{s}}{\widetilde{C}}. \tag{30}$$

We see that this approximation for the change in $\overline{\widetilde{P}}_{\max}$ due to roughness is linear in $\tilde{s}$ (when $\tilde{s}$ is small) and inversely proportional to $\widetilde{C}$. Although we believe this is a reasonable approximation for very small $\tilde{s}$, it is difficult to check, because numerical calculations are inaccurate or impossible because of the behavior of the integrand of Equation (22) for small $\tilde{s}$. When comparing Equation (30) with the numerical calculations we have done, we see that, practically speaking, it becomes accurate only for $\widetilde{C} \geq 10$ when $\tilde{s}$ is of order

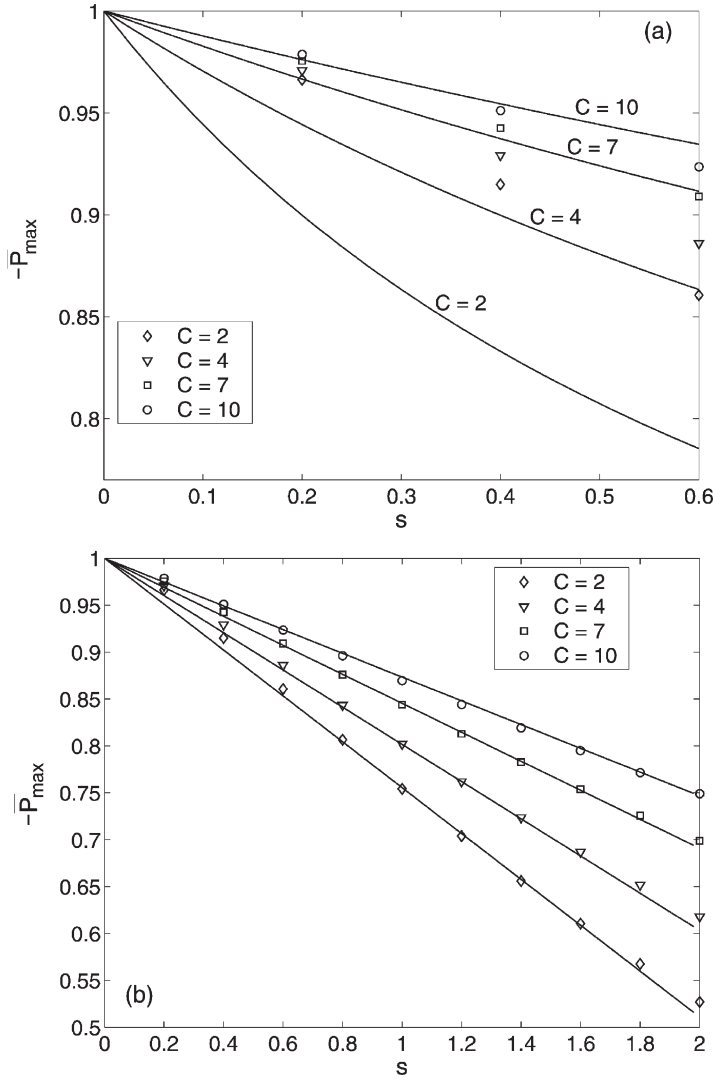

FIGURE 5 Approximations to the peak tensile load in the limit of small fibril height standard deviation, $\tilde{s}$: (a) approximation resulting from bilinear model of $\tilde{\bar{P}}(\tilde{D})$, Equation (30) and (b) phenomenological approximation, Equation (31). Data points are numerical results; solid lines are approximations. All quantities in the plots are normalized; see text for definitions.

0.1. (See Figure 5a for a plot of this comparison.) For this crude bilinear model, we expect little more, especially because its accuracy is poorest in the region of interest (near the pull-off load).

However, using Equation (30) as a guide, we found a phenomenological relationship based on the computations that works well over a larger range of $\tilde{s}$, *i.e.*

$$\overline{\widetilde{P}}_{\max} \approx -1 + \frac{\tilde{s}}{\alpha \widetilde{C} + \pi}, \tag{31}$$

where $\alpha \approx 0.4760$. This model works very well for $\tilde{s} \leq 2$, as long as $\widetilde{C}$ is about order 1 or larger. (See Figure 5b for a plot comparing Equation (31) to the numerical results.)

In addition to this approximation for the pull-off force in the limit of small $\tilde{s}$, a scaling law for the work of separation can be obtained in the limit when $\widetilde{C} \gg \tilde{s}$, which is the ideal case for geckos and other animals. In this limit, the bilinear approximation given previously (Equations (26) and (28)) becomes very good, and $\widetilde{P}_{\max} \to -1$. Skipping the details, it is straightforward to show that the work of separation $\widetilde{U}/\widetilde{\Sigma} \to \widetilde{C}\overline{\widetilde{P}}_{\max}^2/2 = \widetilde{C}/2$ when $\widetilde{C} \gg \tilde{s}$ for the bilinear approximation. In dimensional form, $U \to \Sigma C P_c^2/2$, *i.e.*, the work of separation is dominated by the elastic energy stored in the springs, which is exactly what one expects in the large compliance limit.

By observing Figure 4b, which plots $\widetilde{U}/\widetilde{\Sigma}$ as a function of $\widetilde{C}$ for several values of $\tilde{s}$, it is clear that the approximation $\widetilde{U}/\widetilde{\Sigma} \to \widetilde{C}/2$ does a very good job of predicting the slope of $\widetilde{U}/\widetilde{\Sigma}$ in the proper limit. Indeed, for the case $\tilde{s} = 0$ in that plot, the slope is exactly 1/2. However, although $\widetilde{U}/\widetilde{\Sigma}$ is linear in $\widetilde{C}$ for all cases of $\tilde{s}$ shown, the slope increases by a significant, although small, amount for the other curves. (The slope of the $\tilde{s} = 8$ case is roughly 0.62.) This is to be expected, because the assumption $\widetilde{C} \gg \tilde{s}$ is not well satisfied for the range of data plotted in Figure 4b when $\tilde{s} > 1$. Note also that there is a nonzero constant added to each of the linear fits in Figure 4b that the bilinear model does not capture, so that, in fact

$$\widetilde{U}/\widetilde{\Sigma} \to \widetilde{C}/2 + \beta, \quad \widetilde{C} >> \tilde{s}. \tag{32}$$

In the case when $\tilde{s} = \widetilde{C} = 0$, we can integrate the JKR force displacement relationship to find $\beta \approx 2.22$.

Interpretation of Results Relevant to Biological Setae and Synthetic Mimics Thereof

From all the plots in Figures 2–4 and the foregoing discussion, we see that roughness has a significant effect on the adhesion of a fibrillar

interface. As a practical example of a synthetic fibrillar array that one might fabricate, consider a case in which the fibrils are composed of the rubbery polymer poly(dimethylsiloxane) (PDMS) ($E^* \approx 5$ MPa, $W \approx 50\,\mathrm{mJ/m^2}$) and have a radius of curvature $R = 1\,\mu\mathrm{m}$. In this case, the critical displacement for pull-off $|\delta_c|$ is approximately 35 nm. Thus, for $\widetilde{C} \approx 1$, if the standard deviation in fibril height (roughness height) is 70 nm, the maximal adhesion force is reduced by more than half from its maximum value (Figure 2a, $\tilde{s} = 2$). For roughness-height deviation of more than 200 nm, the adhesion is nearly zero (Figure 2a, $\tilde{s} = 6$).

As we mentioned, these results are for normalized compliance equal to 1. For PDMS, and the R value previously mentioned, $|P_c|/|\delta_c| \approx 6.5\,\mathrm{N/m}$. Also, if we assume the fibrils are cylindrical and oriented normal to the backing and substrate, Equation (1) states that $C = L/(\pi R^2 E)$, so that $\widetilde{C} \approx 1$ corresponds to fibrils of length 1.8 μm. It is quite conceivable to be able to fabricate such PDMS structures using photolithography and molding techniques, as described, *e.g.*, in Reference [3] If the fibril length, L, is increased to 10 μm, which is also possible to fabricate, $C = L/(\pi R^2 E) \approx 0.85\,\mathrm{m/N}$ and $\widetilde{C} \approx 5.6$.

It is clear from both Figure 2b and Figure 3a–c that such an increase in compliance helps to mitigate the effects of roughness. However, compliance does not affect the pull-off load as strongly as roughness, so that a correspondingly larger increase in compliance is required to offset the loss in peak load for increased roughness. This can be accomplished by increasing the mean fibril length, although this cannot be done indefinitely, because fibrils with too great an aspect ratio will adhere to each other laterally, preventing their proper functioning [3]. Another way to increase compliance at a fixed aspect ratio is to orient the fibrils at an angle of $< 90^\circ$ to the backing. The additional compliance supplied by allowing the fibrils to function in bending mode can be quite significant, especially for high aspect ratio fibrils. (See Equation (2).)

Because the compliance is smaller for higher modulus materials such as keratin ($E^* \sim 1\,\mathrm{GPa}$), which composes most biological fibrils, the use of angled fibrils becomes a necessity. Geckos appear to have surmounted the roughness problem in this way. In the case of the tokay gecko (*Gekko gecko*), the fibrils are oriented at an angle of approximately 30° to the substrate at failure [5]. If we consider a setal aspect ratio, $\overline{L}/R$, of 30, which is a conservative estimate for these animals, the compliance is enhanced 1000 times over fibrils oriented normal to the substrate. For keratin with $\overline{L} = 30\,\mu\mathrm{m}$ and $\mathrm{R} = 1\,\mu\mathrm{m}$, the normalized compliance $\widetilde{C} \approx 10$. For an aspect ratio of 100, with $\overline{L} = 100\,\mu\mathrm{m}$ and $R = 1\,\mu\mathrm{m}$, which is not unreasonable based on SEM

studies of gecko setae (see, *e.g.* reference [7]), $\widetilde{C} \approx 370$. Note from the PDMS example that without such large values of compliance, fibrillar adhesion would be poor except on the smoothest of substrates.

We should note here that compliance enhancement as a result of fibrils undergoing a bending mode of deformation is not the only available mechanism biology has employed to overcome roughness. In fact, highly compliant structures are built into most biological adhesion systems at many levels. For instance, in lizards, setae are attached to a flexible membranous backing layer of skin, which is attached to the soft flesh of the toe. At a much smaller scale, a very important means by which nearly all biological setae attain a large amount of contact compliance is through the thin plate-like spatulas found at their ends [11], as mentioned in the introduction. Although the JKR theory is not a good model for adhesion of these structures (see rather Reference [11]), these very flexible plates allow for more setae to make and maintain intimate contact with the substrate.

Before concluding, let us make one final comment about the relevance of our results to biological adhesion. Although both the pull-off stress and work of separation are important quantities for understanding the adhesion performance of a fibrillar interface, the work of separation is likely to be the most critical quantity to lizard adhesion, because we expect detachment to occur by crack propagation from the edge of the toe-substrate contact region in this case. The failure will occur when the stored strain energy in the toe structure available for propagating the crack is greater than the calculated work of separation. Conversely, in the case of insects, the foot pad is much smaller. As a result, one could imagine situations in which all setae on the foot are in a state of equal load sharing. In this case, the pull-off stress would be the most important quantity, and failure would occur when the stress on the fibrils exceeds the critical value.

CONCLUSION

We studied the mechanics of fibrillar adhesion against a rough surface. In our model, the fibrils consisted of linear springs terminated by hemispheres that make JKR adhesive contact with a flat surface. Roughness was modeled by making the fibril length a random variable that follows a continuous probability distribution.

When the fibril length (roughness height) is normally distributed, we found that two parameters determine the mean fibrillar load: the normalized standard deviation in fibril length ($\tilde{s}$) and the normalized fibrillar compliance ($\widetilde{C}$). Full numerical solutions for the mean fibrillar

load as a function of displacement of the fibrillar array, the mean pull-off force, and the work of separation of the fibrillar array were presented for a large range of the parameters $\tilde{s}$ and $\widetilde{C}$. Analytic asymptotic results were given in several limits that confirmed the scaling indicated by the numerical calculations.

Several important conclusions were evident from our analysis. First, the mean fibrillar pull-off force decreases with increasing roughness-height standard deviation. The relationship is linear for small $\tilde{s}$, with the pull-off force trailing off to zero as $\tilde{s}$ is further increased. The effect of increasing compliance is to offset that of roughness; for small $\tilde{s}$, the decrease in pull-off force with increasing $\tilde{s}$ is inversely proportional to $\widetilde{C}$. Moreover, unlike the pull-off force, we found that the fibrillar interfacial work of separation is *constant* for small roughness-height standard deviation and decreases to zero for rougher surfaces. However, similar to the pull-off force, the work of separation increases for increased compliance; in the limit when $\widetilde{C} \gg \tilde{s}$, we found that the work of separation is linearly proportional to $\widetilde{C}$, with slope equal to 1/2. These results were related to recent findings regarding fibrillar adhesion in lizards and insects.

ACKNOWLEDGMENTS

This work was supported in part by start-up funds from Lehigh University for Anand Jagota and by a grant from the DuPont company. All of us are also indebted to Professor Manoj Chaudhury for his pioneering work in this field generally and for many specific and detailed discussions over the years spanning subjects too broad to be enumerated. We offer this in his honor as a small contribution to his vision that, indeed, *biology is mechanics!*

APPENDIX 1

The behavior of $\overline{\widetilde{P}}(\widetilde{D})$ for small values of $\tilde{s}$ can be obtained using the Laplace method. (For a discussion of the Laplace method, see Reference [12].) Let

$$\lambda \equiv 1/(2\tilde{s}^2), \tag{A1}$$

such that $\lambda \to \infty$ as $\tilde{s} \to 0$. We can rewrite Equation (20) as

$$\overline{\widetilde{P}}(\widetilde{D}) = \frac{1}{\sqrt{2\pi}\tilde{s}} \int_1^\infty e^{-\lambda\phi(\tilde{a})} f(\tilde{a}) h(\tilde{a}) d\tilde{a}, \tag{A2}$$

where

$$\phi(\tilde{a}) = \left[\widetilde{D} + \widetilde{C}\tilde{f}(\tilde{a}) + \tilde{g}(\tilde{a})\right]^2. \tag{A3}$$

See also Equations (16)–(18).

The essence of the Laplace method is that the behavior of the integral

$$I(\lambda) \equiv \int_1^\infty e^{-\lambda\phi(\tilde{a})} f(\tilde{a}) h(\tilde{a}) d\tilde{a} \tag{A4}$$

for large λ is completely dictated by the rapid exponential growth of the function $e^{-\lambda\phi(\tilde{a})}$ at the minimum of $\phi(\tilde{a})$. Specifically, if the function $\phi(\tilde{a})$ has a minimum at $\tilde{a} = c \in [1, \infty)$, then it is only the immediate neighborhood of $\tilde{a} = c$ that contributes to the full asymptotic expansion of $I(\lambda)$.

Note that the minimum of $\phi(\tilde{a})$ for $\tilde{a} \in [1, \infty)$ occurs at $\tilde{a} = 1$ if $\widetilde{D} - \widetilde{C} - 1 > 0$. In this case, the function $\phi(\tilde{a})$ is monotonically increasing in $\tilde{a} \geq 1$, so that $d\phi(\tilde{a})/d\tilde{a} > 0$ at $\tilde{a} = 1$. Hence, the inverse function exists, and Equation (A4) is

$$I(\lambda) = \int_1^\infty e^{-\lambda u} F(u) \frac{du}{d\tilde{a}} d\tilde{a}, \tag{A5}$$

where

$$u = \phi(\tilde{a}), \tag{A6a}$$

$$F(u) \equiv f(\tilde{a}(u)) h(\tilde{a}(u)). \tag{A6b}$$

The Laplace method implies that the leading behavior of I(s) is

$$I(\lambda) \approx \left[F(u)\frac{d\tilde{a}}{du}\right]\Big|_{u=\phi(1)} \int_{\phi(1)}^\infty e^{-\lambda u} du = \left[F(u)\frac{d\tilde{a}}{du}\right]\Big|_{u=\phi(1)} \frac{e^{-\lambda\phi(1)}}{\lambda}. \tag{A7}$$

Note that

$$\left[F(u)\frac{d\tilde{a}}{du}\right]\Big|_{u=\phi(1)} = \frac{f(1)h(1)}{\left(\frac{du}{d\tilde{a}}\right)_{\tilde{a}=1}}. \tag{A8}$$

Further more,

$$\phi(1) = (\widetilde{D} - \widetilde{C} - 1)^2, \tag{A9a}$$

$$f(1)h(1) = -4, \tag{A9b}$$

$$\left(\frac{du}{d\tilde{a}}\right)_{\tilde{a}=1} = 8(\widetilde{D} - \widetilde{C} - 1), \tag{A9c}$$

and, thus,

$$I(\lambda) = -\frac{\exp[-\lambda(\widetilde{D} - \widetilde{C} - 1)^2]}{2\lambda(\widetilde{D} - \widetilde{C} - 1)} \tag{A10}$$

and

$$\overline{\widetilde{P}}(\widetilde{D}) = -\frac{\tilde{s}\exp[-(\widetilde{D} - \widetilde{C} - 1)^2/(2\tilde{s}^2)]}{\sqrt{2\pi}(\widetilde{D} - \widetilde{C} - 1)}. \tag{A11}$$

In other words, if $(\widetilde{D} - \widetilde{C} - 1)/\tilde{s} \gg 1$, Equation (A11) implies that the load is exponentially small. The load is significantly only if $\widetilde{D} \cong \widetilde{C} + 1$. However, Equation (A11) is not valid if $\widetilde{D} - \widetilde{C} - 1 = 0$, because $d\phi(\tilde{a})/d\tilde{a} = 0$ at $\tilde{a} = 1$ when this is true. Our assumptions are violated in this case, and Equation (A8) is not valid.

To investigate the load when $\widetilde{D} \cong \widetilde{C} + 1$, we modify the Laplace method by writing a Taylor series for $\phi(\tilde{a})$ about the point $\tilde{a} = 1$. Letting $\varepsilon \equiv \widetilde{D} - \widetilde{C} - 1$, one has

$$\phi(\tilde{a}) \approx \varepsilon^2 + 8\varepsilon(\tilde{a} - 1) + [16 + (7 + 9\widetilde{C}/2)\varepsilon](\tilde{a} - 1)^2. \tag{A12}$$

Because ε is small, we let

$$\phi(\tilde{a}) \approx \varepsilon^2 + 8\varepsilon(\tilde{a} - 1) + 16(\tilde{a} - 1)^2 = [4(\tilde{a} - 1) + \varepsilon]^2. \tag{A13}$$

This approximation for $\phi(\tilde{a})$ has a minimum at

$$\tilde{a} = \tilde{a}^* \equiv 1 - \varepsilon/4. \tag{A14}$$

When $\varepsilon < 0$, the minimum of $\phi(\tilde{a})$ for $\tilde{a} \in [1, \infty)$ does not occur at $\tilde{a} = 1$ but occurs rather at $\tilde{a} = \tilde{a}^*$ for small ε. Note that we are most interested in the case $|\varepsilon| \ll 1$ and $\varepsilon < 0$, because the maximum in $\overline{\widetilde{P}}(\widetilde{D})$ occurs at $\widetilde{D}$ just less than $\widetilde{C} + 1$ for small $\tilde{s}$. (See Figure 2.) For the rest of this calculation, we focus on the situation where $|\varepsilon| \ll 1$ and $\varepsilon < 0$.

Equation (A2) becomes

$$\begin{aligned}\overline{\widetilde{P}}(\widetilde{D}) &\approx \frac{1}{\sqrt{2\pi}\tilde{s}}\int_1^\infty e^{-\lambda[4(\tilde{a}-1)+\varepsilon]^2} f(\tilde{a})h(\tilde{a})d\tilde{a} \\ &\approx \frac{f(\tilde{a}^*)h(\tilde{a}^*)}{\sqrt{2\pi}\tilde{s}}\int_0^\infty e^{-\lambda[4\nu+\varepsilon]^2} d\nu.\end{aligned} \tag{A15}$$

If we let $w = 4\nu + \varepsilon$ and $x = w\sqrt{\lambda}$, then

$$\overline{\widetilde{P}}(\widetilde{D}) \approx \frac{f(\tilde{a}^*)h(\tilde{a}^*)}{4\sqrt{2\pi\tilde{s}}} \int_{\varepsilon}^{\infty} e^{-\lambda w^2} dw = \frac{f(\tilde{a}^*)h(\tilde{a}^*)}{4\sqrt{2\pi\lambda\tilde{s}}} \int_{\varepsilon\sqrt{\lambda}}^{\infty} e^{-x^2} dx. \tag{A16}$$

The integral can be evaluated, and one has

$$\overline{\widetilde{P}}(\widetilde{D}) \approx \frac{f(\tilde{a}^*)h(\tilde{a}^*)}{8} \operatorname{erfc}\left(\frac{\widetilde{D} - \widetilde{C} - 1}{\sqrt{2\tilde{s}}}\right), \tag{A17}$$

where erfc is the complementary error function. Note that when $\varepsilon > 0$ and $|\varepsilon| << 1$, Equation (A17) is still a valid approximation, as long as one sets $\tilde{a}^* = 1$.

In the limit when $\tilde{s} \to 0$, the maximum mean load will occur closer and closer to the point $\widetilde{D} = \widetilde{C} + 1$. Now, when $\widetilde{D} = \widetilde{C} + 1$, we know that the minimum in $\phi(\tilde{a})$ occurs at $\tilde{a} = 1$. Likewise, for the approximation to $\phi(\tilde{a})$, $\tilde{a}^* \to 1$. Hence, in the small $\tilde{s}$ limit, a good approximation to (A17) is

$$\overline{\widetilde{P}}(\widetilde{D}) \approx \frac{f(1)h(1)}{8} \operatorname{erfc}\left(\frac{\widetilde{D} - \widetilde{C} - 1}{\sqrt{2\tilde{s}}}\right) = -\frac{1}{2} \operatorname{erfc}\left(\frac{\widetilde{D} - \widetilde{C} - 1}{\sqrt{2\tilde{s}}}\right). \tag{A18}$$

Now, for small $\tilde{s}$ and $\widetilde{D}$ less than $\widetilde{C} + 1$, Equation (A18) predicts $\overline{\widetilde{P}}(\widetilde{D}) \to -\operatorname{erfc}(-\infty)/2 = -1$**. That is $\overline{P} \to P_c$, where P_c is the JKR failure load. This is just what we expect, because all the fibrils will fail at the same time, *i.e.*, when the JKR failure load is reached, for no length variation. Unfortunately, because $\overline{\widetilde{P}}(\widetilde{D}) = -1$ effectively for all $\widetilde{D} < \widetilde{C} + 1$, Equation (A18) does not allow one to determine the scaling of the maximum tensile load with $\tilde{s}$ at small $\tilde{s}$. This is true because Equation (A18) is valid only for $\widetilde{D}$ close to $\widetilde{C} + 1$. However, by a simple physical argument, one may approximate $\overline{\widetilde{P}}(\widetilde{D})$ for smaller $\widetilde{D}$; this allows one to extract the scaling of $\max[-\overline{\widetilde{P}}(\widetilde{D})]$ with $\tilde{s}$ and $\widetilde{C}$ at small $\tilde{s}$. See the discussion section in the main text.

**Note that $\overline{\widetilde{P}}(\widetilde{D})$ goes to -1 rather than $+1$ as shown in Figures 2 and 3 because we did not change the sign of $\widetilde{P}$ here, as we did in those figures. (Note the contact mechanics convention that negative forces are tensile, which is opposite to the usual solid mechanics convention.)

REFERENCES

[1] Persson, B. N. J., *J. Chem. Phys.* **118**, 7614–7621 (2003).
[2] Arzt, E., Gorb, S., and Spolenak, R., *Proc. Natl. Acad. Sci. USA* **100**, 10603–10606 (2003).
[3] Glassmaker, N. J., Jagota, A., Hui, C.-Y., and Kim, J., *J. Royal Society, Interface* **1**, 23–33 (2004).
[4] Hui, C.-Y., Glassmaker, N. J., Tang, T., and Jagota, A., *J. Royal Society, Interface* **1**, 35–48 (2004).
[5] Autumn, K., Yiching, A., Liang, S., Hsieh, T., Zesch, W., Chan, W. P., Kenny, T. W., Fearing, R., and Full, R. J., *Nature* **405**, 681–685 (2000).
[6] Eisner, T. and Aneshansley, D. J., *Proc. Natl. Acad. Sci. USA* **97**, 6568–6573 (2000).
[7] Ruibal, R. and Ernst, V., *J. Morph.* **117**, 271–294 (1965).
[8] Glassmaker, N. J., Jagota, A., and Hui, C.-Y., Adhesion enhancement in a synthetic fibrillar interface *Acta Biomaterialia*, **1**, 367–375 (2005).
[9] Greenwood, J. A. and Williamson, J. B., *Proc. R. Soc. London, Ser. A* **295**, 300–319 (1966).
[10] Johnson, K. L., Kendall, K., and Roberts, A. D., *Proc. R. Soc. London, Ser. A* **324**, 301–313 (1971).
[11] Persson, B. N. J. and Gorb, S., *J. Chem. Phys.* **118**, 11437–11444 (2003).
[12] Carrier, G. F., Krook, M., and Pearson, C. E., *Functions of a Complex Variable—Theory and Techniques* (McGraw-Hill, New York, 1966).